CLAS-NOTE-92-009

CONTINUOUS ELECTRON BEAM ACCELERATOR FACILITY

PHOTOMULTIPLIERS FOR THE ELECTROMAGNETIC SHOWER CALORIMETER OF THE CEBAF LARGE ACCEPTANCE SPECTROMETER

V.Burkert[1], Yu.Efremenko[2], K.Egiyan[4], K.Giovanetti[3], V. Gavrilov[2], H.Mkrtchan[4], E.Smith[1], S.Stepanyan[4]

[1] CEBAF, Newport News, Va, USA

[2] ITEP, Moscow, Russia

[3] James Madison University, Harrisonburg, Va, USA

[4] YerPI, Yerevan, Armenia

Contents

1 Introduction 3

2 The Calorimeter 3
- 2.1 Overview 3
- 2.2 Photomultiplier Tube Specifications 4

3 Photomultiplier Tube Tests 6
- 3.1 Test Setup 7
- 3.2 Results 13

4 Conclusion 23

A TOF Measurement for Neutrons 24

B Acknowledgements 26

1 Introduction

Particles produced in electron nucleus scattering experiments in Hall B at CEBAF will be measured by the detector subsystems of the CEBAF Large Acceptance Spectrometer, CLAS. One of the CLAS detector subsystems is the forward electromagnetic calorimeter [1,2]. This calorimeter will be used to enhance particle identification by distinguishing pions from electrons. In addition, the detector has been designed to enable the detection of neutral particles, specifically photons and neutrons. This detector subsystem is referred to as the EMC, electromagnetic calorimeter. This report will summarize the results of tests of photomultiplier tubes for use in the readout of the EMC detector. The report gives a brief overview of the EMC detector with emphasis on those characteristics which place constraints on the performance of the photomultiplier tubes, followed by an evaluation of various photomultiplier tubes.

2 The Calorimeter

2.1 Overview

The CLAS detector is divided into six sectors. The forward part (8°-45°) of each of the six CLAS sectors will be equipped with an independent electromagnetic shower calorimeter having an approximate triangular shape. Each calorimeter consist of 13 similar submodules, each submodule having 3 layers of 2.2 mm thick lead plates interleaved with 10 mm thick, roughly 10 cm wide scintillators. The scintillator strips in consecutive layers are rotated by approximately 120 degrees with respect to the previous plane. The three orientations are labeled U, V and W. The U, V and W readout provides stereo information on the location of any energy deposition. Each scintillation layer consist of 36 scintillator strips. The inner, (5 submodules) and outer (8 submodules) sections of calorimeter are read out independently. The system thus requires a total of 6x3x36x2=1296 photomultiplier tubes, PMTs. In order for the scintillators in any submodule to subtend the same target solid angle, the lengths and widths of the scintillators gradually increase from the inner to the outermost scintillator.

High energy electrons, positrons and photons generate electromagnetic

showers in the calorimeters. The energy in these showers is sampled in the scintillation layers. Heavy charged particles, for example pions and nucleons, will lose energy both through ionization and through hadronic interactions (hadronic showers). Neutrons will be detected by detecting the charged by-products from hadronic interactions. In order to evaluate the performance of candidate photomultiplier tubes, specific performance criteria have been established. These are related to particle detection goals and some assumed performance levels for detector components. Table 1 summarizes detector characteristics of interest, and Table 2 gives the corresponding requirements for the PMT of choice.

2.2 Photomultiplier Tube Specifications

Energy resolution for an electromagnetic shower is predominantly determined by a combination of shower fluctuations, shower leakage and photoelectron statistics. The EMC detectors have been designed to have photon and electron energy resolutions of better than $10\%/\sqrt{E(GeV)}$ for energies up to 4 GeV. To insure that the energy resolution is not significantly affected by photoelectron statistics a minimum of 5 photoelectrons/MeV is desired. This number represents the average number of photoelectrons, pe's, produced at the photomultiplier tube per MeV of deposited energy in the scintillator when there are no attenuation losses. For a given deposited energy, the number of photoelectrons will vary due to attenuation of the light in the scintillator. [a]

The necessary dynamic range of the readout system can be estimated by comparing the average energy deposition of a minimum ionizing particle, MIP, with the maximal energy deposition of a 6 GeV electron. For a MIP, an average of 10 MeV (16 MeV) will be deposited along the 5 cm (8 cm) path through an inner (outer) section. The attenuation of this signal in the longest scintillator (4.5 m) is .22. The attenuated signal, therefore, has an equivalent energy deposition of 2.2 MeV or 11 pe. At the other extreme, a 6 GeV electron may deposit up to 450 MeV in an inner submodule. For this estimate, the electron is assumed to deposit 2/3 of its energy in the

[a] An attenuation length of three meters has been assumed for the estimates made in this report. This value is consistent with measured attenuations with optical fiber readout of the EMC.

forward part of the calorimeter with equal distribution of the energy among the three orientations (U, V and W), transverse shower spreading has been ignored, and a sampling fraction of 1/3 [b] has been used to estimate the energy deposited in the scintillator. The desired range of linearity for the readout has been chosen to extend from 1 to 3500 pe's in order to amply include these extremes and account for the possibility of higher sensitivity for some readout channels (8 pe/MeV). A 10 bit ADC (1024 channels) for each readout channel with a sensitivity of .25 pC/channel will be used to measure the integrated signal.

In order to use MIP's to calibrate the energy and time measurements of the EMC, discriminator thresholds must be set to be fully efficient for these energy losses. A particle that passes through a scintillator at the maximum distance from the readout end should produce a signal large enough to trigger the timing discriminator. For an MIP this results in the light equivalent of a 2.2 MeV (11 pe's). If a 20 mV threshold is used for the timing discriminator then an 11 pe signal should produce a 50 mV average pulse in order to have considerable chance of triggering the timing circuitry. The integrated charge in a 30 ns PMT pulse is roughly 1/2 base (30 ns) times the height (Vo/R). These assumptions predict a 15.4 pC integrated charge for a 50 mV voltage amplitude across a 50 ohm load. A PMT gain of 8.5 x 10^6 will increase the 11 pe's on the cathode to the required 15.4 pC at the anode. A minimal gain of 1x10^7 is required of the PMTs. If this signal is to be applied to the input of a 10 bit .25 pC/channel ADC, an attenuation factor of 22 dB is required in order to insure that the largest outputs remain within the ADC range.

The required time resolution of the EMC detector can be estimated by considering neutron detection. Time of flight, TOF, will be used to determine the velocity of detected neutrons. A velocity measurement will be used both to determine neutron energies and separate neutrons from photons. The error in the measured velocity is due to the uncertainty in the flight path and the flight time [3,4,5]. Flight path uncertainty results from an inability to determine the longitudinal location of the neutron interaction [c] in the detector. The maximum in longitudinal uncertainty is

[b] The factor 1/3 is in agreement with the results of GEANT and EGS simulations.

[c] Transverse refers to the direction parallel to the front layer while longitudinal refers to the direction perpendicular.

.29 m. This occurs when the point of interaction is in the outer section of the detector and is completely unknown. This uncertainty in the flight path is approximately 5% of the typical flight path to the EMC detector. If the points of interaction are distributed uniformly in the longitudinal direction then, σ_{path}, the rms deviation, would be 1.5%. The combination of the variation in the neutron interaction and the geometry of the EMC detector complicate the analysis of the TOF error. A brief but more complete discussion can be found in the appendix (section A). Based on these considerations and on experience gained in testing an EMC prototype a design goal of $\sigma = 400ps$ is consistent with the time specifications of the EMC detector.

Table 1: Characteristics of EMC Detector

Detector *Characteristic*	*Design Goal*
Energy Resolution (%)	$9/\sqrt{E}$
Photoelectrons per MeV	5 pe/ MeV
Operating Range	10 MeV - 6 GeV electron
Operating Range (Sampled Energy)	.5-450 MeV
Time Resolution σ	$\leq$400 ps
Scintillator Lengths	0.15 - 4.5 m
Flight Path Uncertainty	.29 m
Target - Detector Distance	5.5 m

3 Photomultiplier Tube Tests

PMT performance was benchmarked against the criteria established above. Tests were performed on several candidate PMTs. When possible more than one PMT of a given variety was tested. Concurrent with photomultiplier tube testing, a redesign of the readout system was undertaken. The original readout, WLS method, uses wavelength shifting readout bars to transport

Table 2: Characteristics of EMC Photomultiplier tubes

Photomultiplier Tubes *Characteristic*	*Specifications*
Operating Range (pe's)	4-3500
Gain	1×10^7
Linearity	1%
Threshold	11 pe
Threshold (MeV equivalent)	2.2 MeV
Gain	$\geq 8.5 \times 10^6$
Time Resolution	$\sigma \leq 400$ ps

the light from the 5 (8) scintillators in a inner (outer) section to the PMTs. A second method employing large diameter polystyrene optical fibers, fiber method, to transport the light is under development. PMTs were therefore tested using both WLS and fiber readout methods. The details of the two systems can be found elsewhere [6].

3.1 Test Setup

Two series of tests, one for each readout method, were used to evaluate the performance of PMTs. Each series of tests relied on two test setups. Figures 1, 2 show the two setups with WLS readout. Both setups were also used with 30 2mm diameter optical fibers in place of the wavelength shifter and light guide. The test were performed in a light tight box. The fibers or WLS were fixed in place. PMTs could easily be changed and tested. In both test setups a light pulse was generated in a scintillator and measured by two PMTs, the one under test (tested PMT) and monitor PMT. The monitor was calibrated and used as a reference.

To evaluate the absolute response of the system in terms of pe/MeV a ^{207}Bi source [7] was used to deposit energy in the scintillator. A typical spectrum as viewed by the monitor PMT is shown in Figure 3. This histogram is labeled as monitor amplitude. The peak is due to a 1 MeV

Figure 1: PMT Test Setup 1

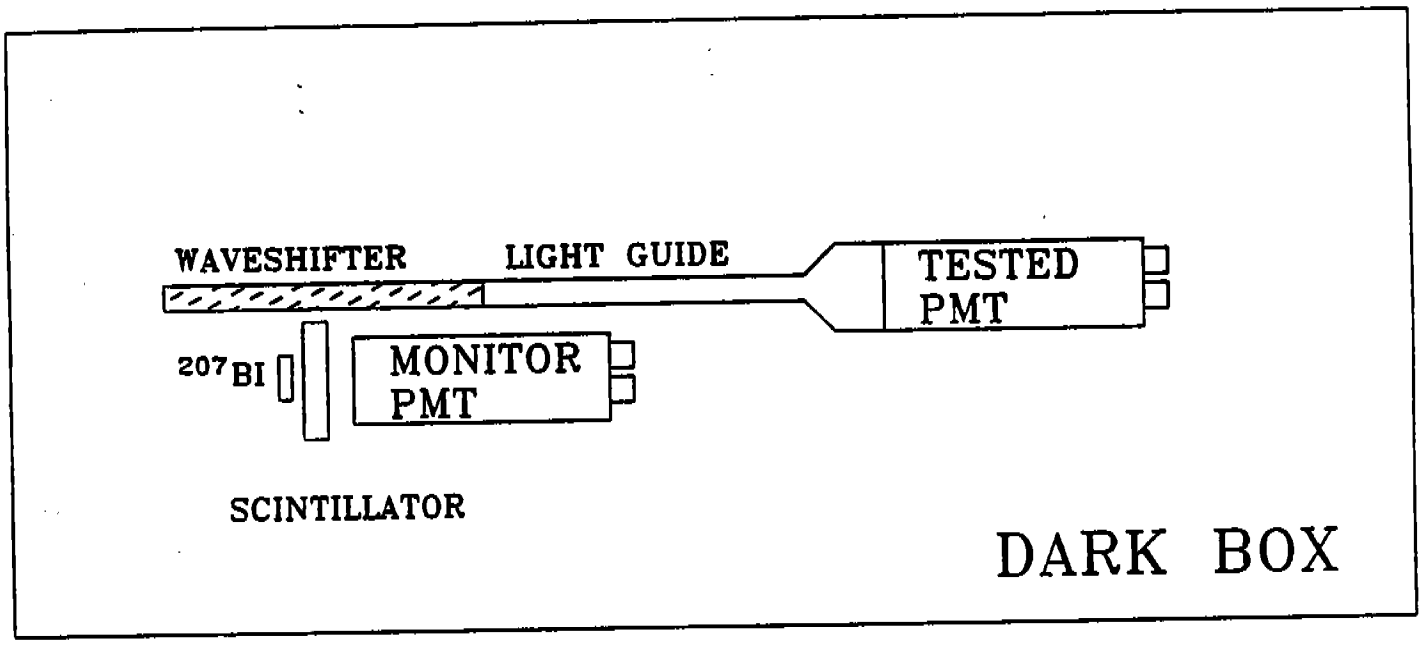

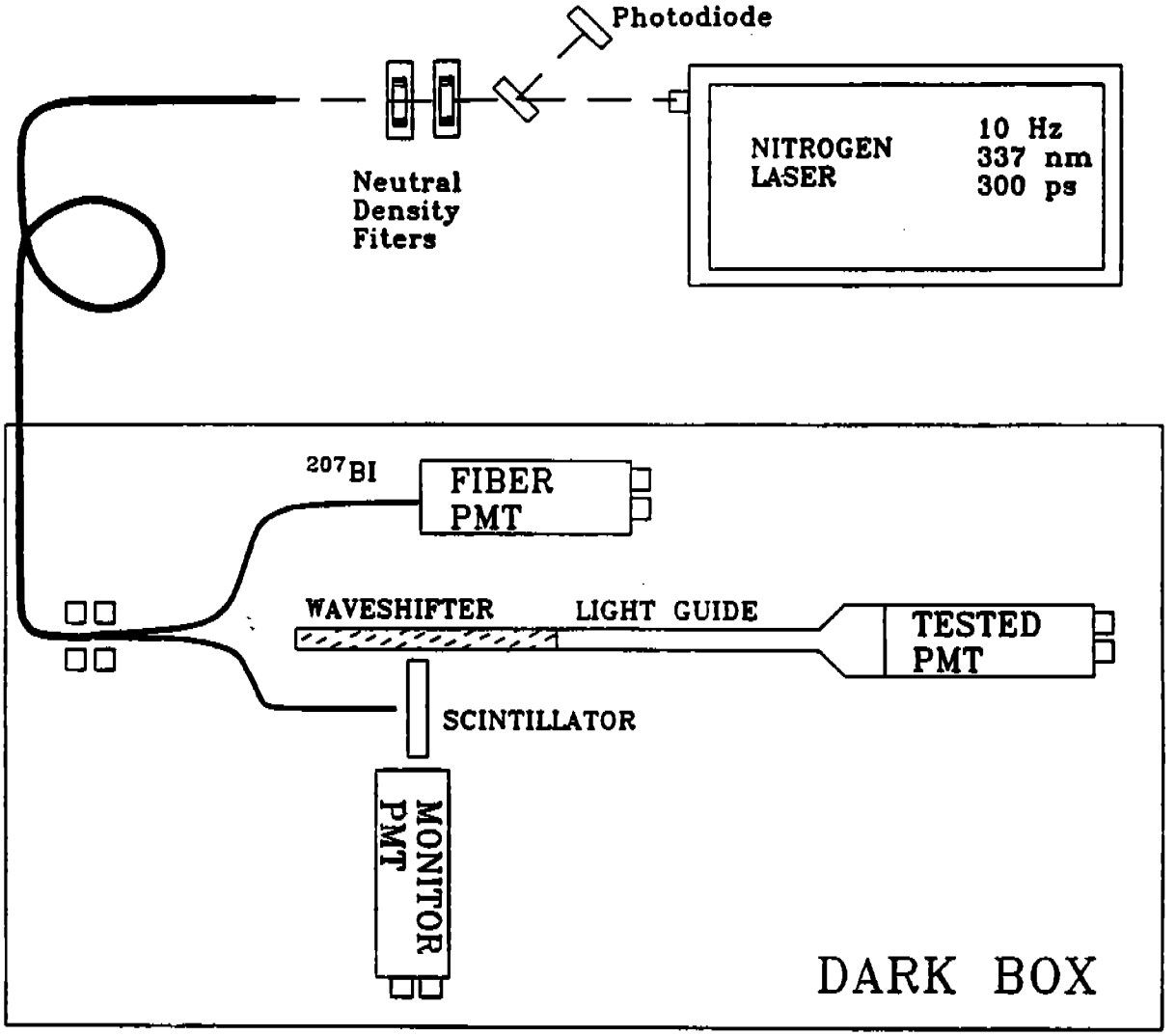

Figure 2: PMT Test Setup 2

K-shell conversion electron. The range of a electron is 30 mm. The response of the tested PMT to 1 MeV of deposited energy is determined by examining events in the test PMT that appear in the peak of the monitor spectrum. An example of three test PMT spectra, one showing full response and two others showing the response to 1 MeV and 0.5 MeV as determined by cuts on the monitor spectrum, are also shown in Figure 3. Two methods were employed to determine the number of pe's. The first method involved fitting the observed spectra to a function, F.

$$F = N_o(e^{-\mu} + \sum_{n=1}^{13}(\frac{\mu^n}{n!}e^{-\mu})(\frac{1}{\sqrt{2n\pi\sigma}}e^{-\frac{1}{2}\frac{(x-(pe0+n\Delta))^2}{n\sigma^2}}))$$

This function describes the spectrum using a sum of Poisson distributions that accounted for the probabilities for 0 pe's, 1 pe, 2 pe's up to 13 pe's. The function was characterized by 4 variables: the mean number of pe's (μ), amplitude (N_o), resolution (σ), and gain (Δ). The second method compared the total number of events in the spectrum with the number of events in the pedestal. If all pedestal events are interpreted as 0 pe events then this ratio can be used to calculate the average number of pe's. When compared both methods estimated the average number of pe's to within 10% of each other. This allowed an absolute calibration of the tested PMT.

To study the response of the PMT over a large dynamic range test setup 2 was used. A nitrogen laser generated a pulse of ultraviolet light. Characteristics of the laser are summarized in Table 3. The laser pulse was transported by optical fibers to two scintillators. One of the scintillators was viewed by the fiber PMT. The other scintillator was viewed by the monitor PMT and the tested PMT. The scintillator and the tested PMT remain in the the same positions as in test setup 1. The monitor PMT was moved to the side where less light reached the PMT.

An UV light pulse generates a response in a scintillator very similar to that of a charged particle. By varying the laser intensity the number of photons created in the scintillator could be varied. The intensity of UV light was adjusted by changing neutral density filters that were mounted in a manually rotatable wheel. The possible attenuation of the laser pulse ranged from 1 dB to 43 dB. Most PMTs were tested over the smaller range,

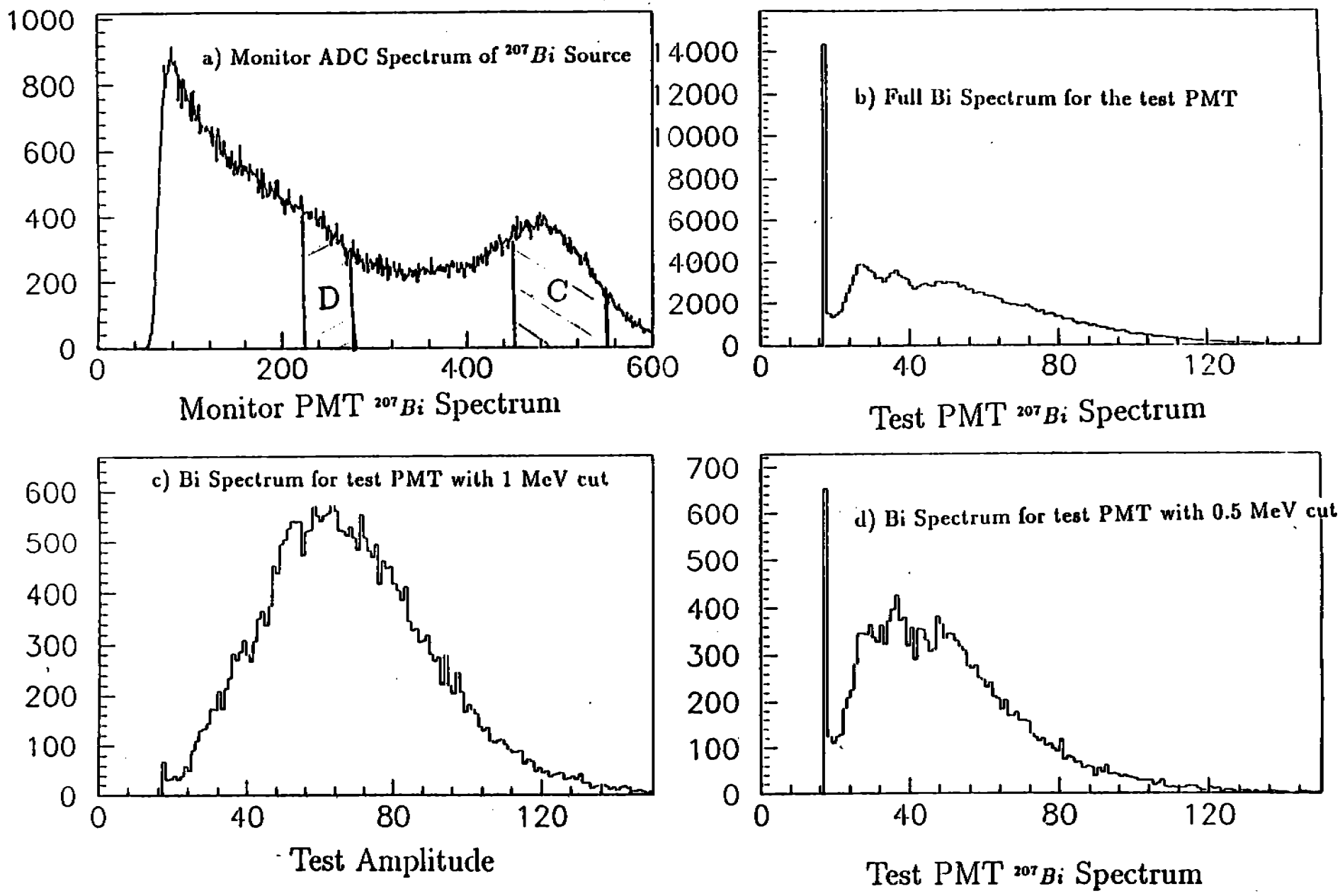
a) Monitor ADC Spectrum of ^{207}Bi Source
D
C
Monitor PMT ^{207}Bi Spectrum
b) Full Bi Spectrum for the test PMT
Test PMT ^{207}Bi Spectrum
c) Bi Spectrum for test PMT with 1 MeV cut
Test Amplitude
d) Bi Spectrum for test PMT with 0.5 MeV cut
Test PMT ^{207}Bi Spectrum

Figure 3:

35 dB to 9 dB. Before passing through the filters, part of the pulse was reflected by a splitting mirror onto a UV sensitive diode. The resulting diode signal was put into a constant fraction discriminator and used to generate the ADC gates as well as the TDC start. The influence of the diode pulse on the timing spectrum was small, independent of the filter wheel setting. Measured σ's as small as 100 ps indicate that the diode timing was no worse than 100 ps.

The absolute calibration obtained for the tested PMT in setup 1 was transferred to the monitor PMT in its new location in setup 2. The amount of measured light for the monitor PMT then served to measure the number of pe's for the tested PMT.

Table 3: Characteristics of the Nitrogen Laser

Energy per Pulse	70 μJ
Pulse Duration	300 ps
Wavelength	337 nm
Photons per Pulse	10^{14}
Repetition Rate	1-20 Hz

During the testing period, tests were run to measure the laser stability. Figure 4 shows how the laser intensity varied over 30hours. The variation of several percent is consistent with manufacturers claims. Over the course of 2 months there was a gradual reduction of the laser intensity by a factor of 2. This was due to a build up of contaminants in the lasing cavity (white powder). A thorough cleaning of the cavity restored the laser. The pulse to pulse variation of the laser was much to large to allow for a measurement of the resolution of the PMT. There was a strong correlation among the PMTs for the measured intensities of a given laser pulse. This correlation is illustrated in the histogram shown in Figure 5. The top three histograms show the lack of correlation between the diode measured intensity and the PMT measured intensity. In contrast the bottom three histograms exhibit a strong correlation between measured laser intensity per pulse. Raw and corrected data for the tested PMT are shown in Figure 6. The tested PMT was corrected by multiplying its measured amplitude by the average

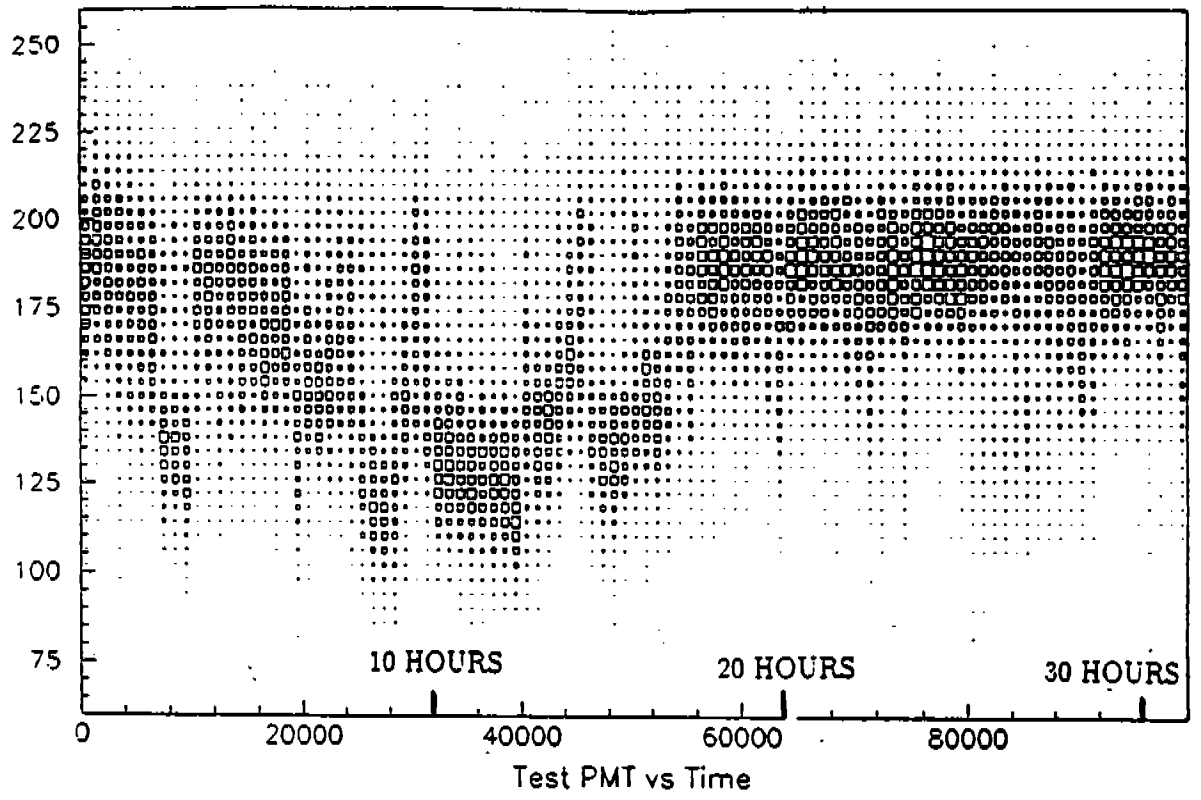

Figure 4: Laser Stability

value of the monitor amplitude divided by the monitor amplitude for that event. The same correction could be applied using the fiber amplitude or a combination of the monitor and the fiber. The correlation between the photodiode amplitude and the other PMTs was much smaller. This is probably due to the variation in the amount of light launched into the fiber. Collimating of the reflected laser pulse did not seem to increase the correlation.

3.2 Results

The first series of tests were done between August 1991 and September 1991 and used the WLS method for readout. The WLS configuration is

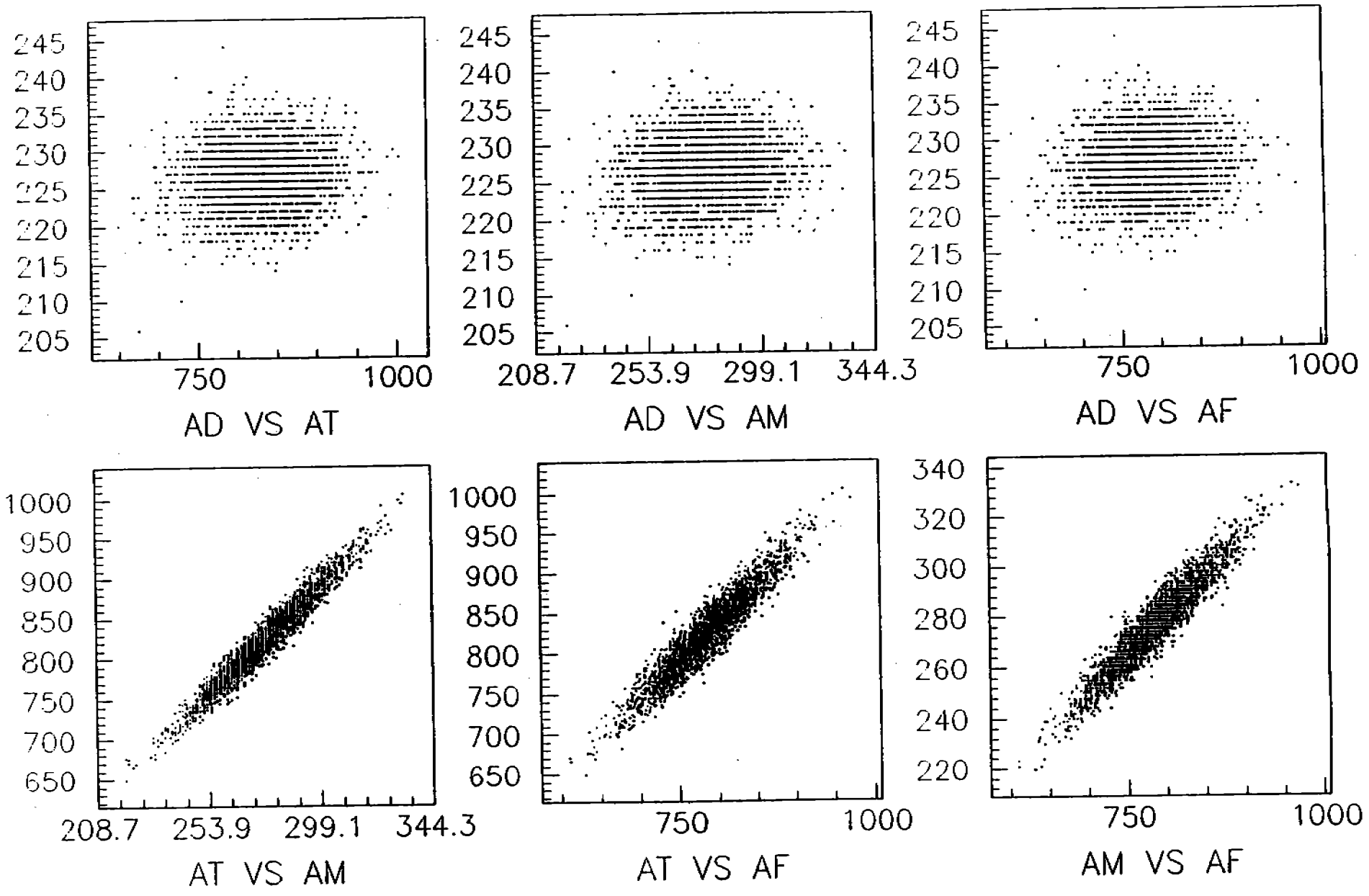

AD=Amplitude of Diode, AT=Amplitude of Test PMT, AF=Fiber PMT, AM=Monitor PMT.

Figure 5: Measured Laser Intensity

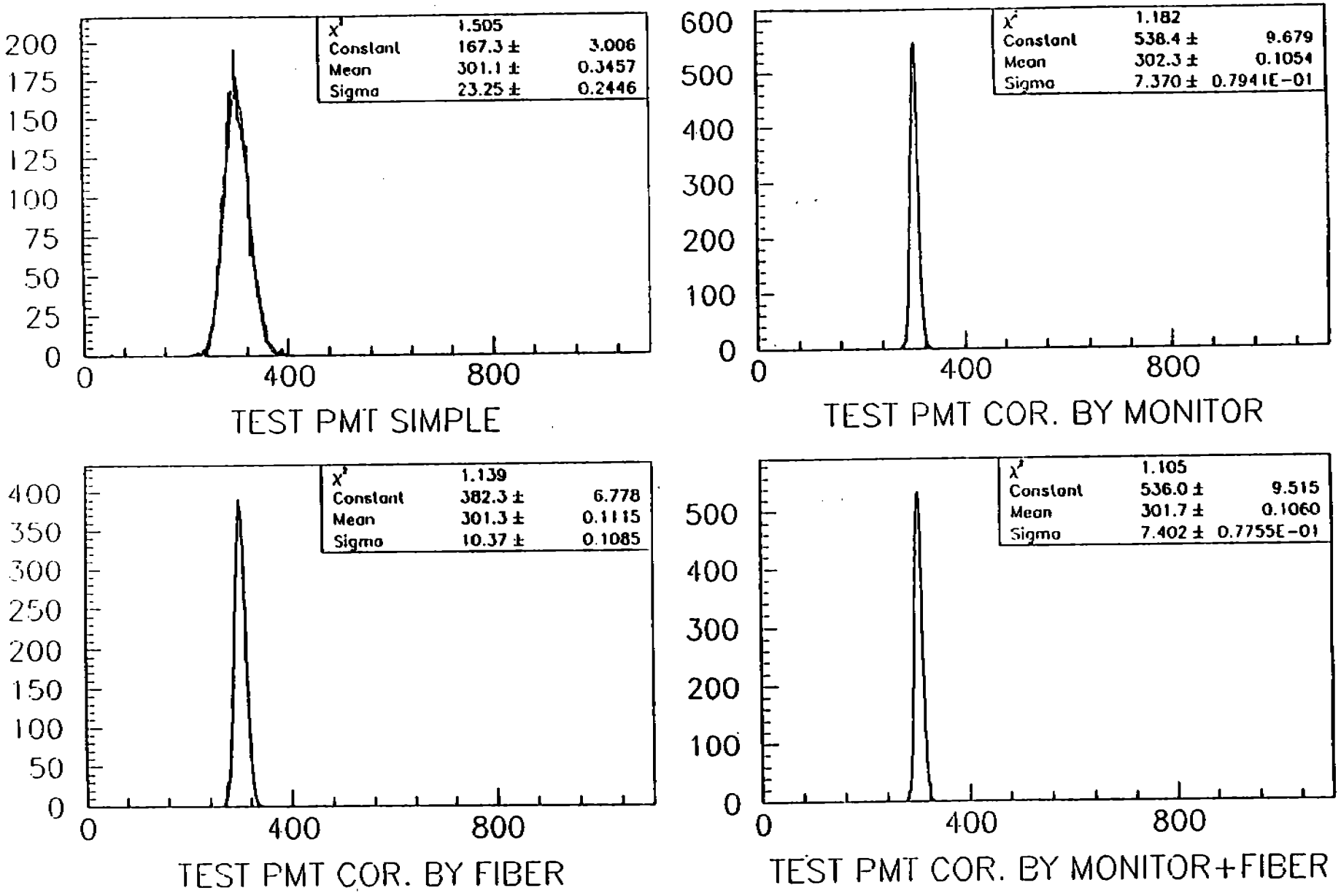

Figure 6: Raw and Corrected Data

shown in the Figures 1,2 [d]. An air gap separated the scintillator and the wavelengthshifter. The PMT was coupled through a clear plexiglass light guide. A sheet of paper was used to block light from directly reaching the PMT from the scintillator. Also light was blocked from hitting the WLS except in the immediate vicinity of the scintillator. The tubes that were tested are listed in Table 4. When possible more than one tube of a given type was tested. A sample of some typical results is shown in Figures 7,8,9,10. For each intensity setting, the amplitude, time, amplitude resolution and time resolution could be measured and are given in the figures. The results for the amplitude resolution were obtained after the amplitude was corrected for the shifts in the laser intensity. The range of intensities was repeated for several high voltage values. The results are summarized in Table 4. A qualitative grade of excellent through poor has been assigned based on the linearity of the response to changing intensity. A parameterization of the time and energy resolution as a function of the number of photoelectron is also given in the table. The functional form for both parameterizations are the same.

$$Function = \sqrt{(\frac{A_1}{\sqrt{N_{pe}}})^2 + (A_2)^2}$$

For the amplitude resolution the parameterization is σ in percent. For the time resolution the parameterization is σ in nanoseconds. The number of pe's/MeV as determined via test setup 2 is also included in the table.

A similar set of PMTs was tested again in October-November. During these tests the fiber readout method was used. Thirty 2mm diameter polystyrene fibers with acrylic cladding were coupled to the end of the scintillator. The fibers were approximately 50 cm long and were bent by 90° with approximately 1" radius of curvature. This design complies with the restriction imposed by the limited available space for the readout. The testing was identical and the results are shown tabulated in Table 5. The table presents the results in the same format as in the WLS case.

Table 6 shows a rough comparison for the light losses of the two readout

[d] The wavelengthshifter used in these tests was Bicron G2.

TESTED TUBES

WAVELEGTH SHIFTER READOUT METHOD

Type	N-stage	Rise time ns	Linearity	N Ph-e, from 1 MeV Accuracy - 20 %	Time res. ns A1	Time res. ns A2	Ampl res. A1	Ampl res. A2	HV
---------- PHILIPS ----------									
XP 2212 (1)	12	4.0	E.....	6.0	3.931	0.106	1.341	0.0061	1550
XP 2212 (2)	12	4.0	E.....	6.0	3.613	0.089	1.281	0.0067	1550
XP 2262 (1) CERN B	12	2.0	..G....	5.0	1.171	0.147	1.241	0.0050	1600
XP 2262 (1)	12	2.0	..G....	5.0	1.543	0.115	1.233	0.0001	1550
XP 2262 (2)	12	2.0	..G....	5.0	1.856	0.063	1.282	0.0110	1550
XP 2020	12	1.5	....F..	5.0	1.805	0.070	1.053	0.0110	1750
XP 2282	8	1.5	..G....	4.0	2.196	0.045	1.010	0.0120	2050
---------- HAMAMATSU ----------									
H 1161 (1)	12	2.7	..G....	9.0	1.873	0.052	1.511	0.011	1450
H 1161 (2)	12	2.7	..G....	9.0	1.843	0.055	1.384	0.011	1450
H 1949 (1)	12	1.3	E.....	8.0	1.802	0.055	1.440	0.009	1550
H 1949 (2)	12	1.3	E.....	8.0	1.733	0.059	1.339	0.011	1550
H 2431 (1)	8	0.7	.....P	9.0	1.705	0.055	1.092	0.002	1800
H 2431 (2)	8	0.7	.....P	9.0	1.841	0.054	1.153	0.023	1800
H 3178 (1) 1.5 inch	10	2.7	E.....	10.0	2.619	0.072	1.354	0.009	1450
H 3178 (2) 1.5 inch	10	2.7	E.....	10.0	2.619	0.089	1.344	0.008	1450
---------- EMI ----------									
9954 [illegible]	12		..G....	5.0	1.816	0.084	1.228	0.011	1750
---------- BURLE ----------									
8575	12	2.8	.....P	5.0	2.021	0.054	1.081	0.018	1400

E - excelent, G - good, F - fair, P - poor.

Table 4: Tabulated Results for the WLS Readout Tests

Amplitude vs # Photoelectrons (WLS Readout, PMT=XP2262)

Amplitude corrected by Monitor PMT

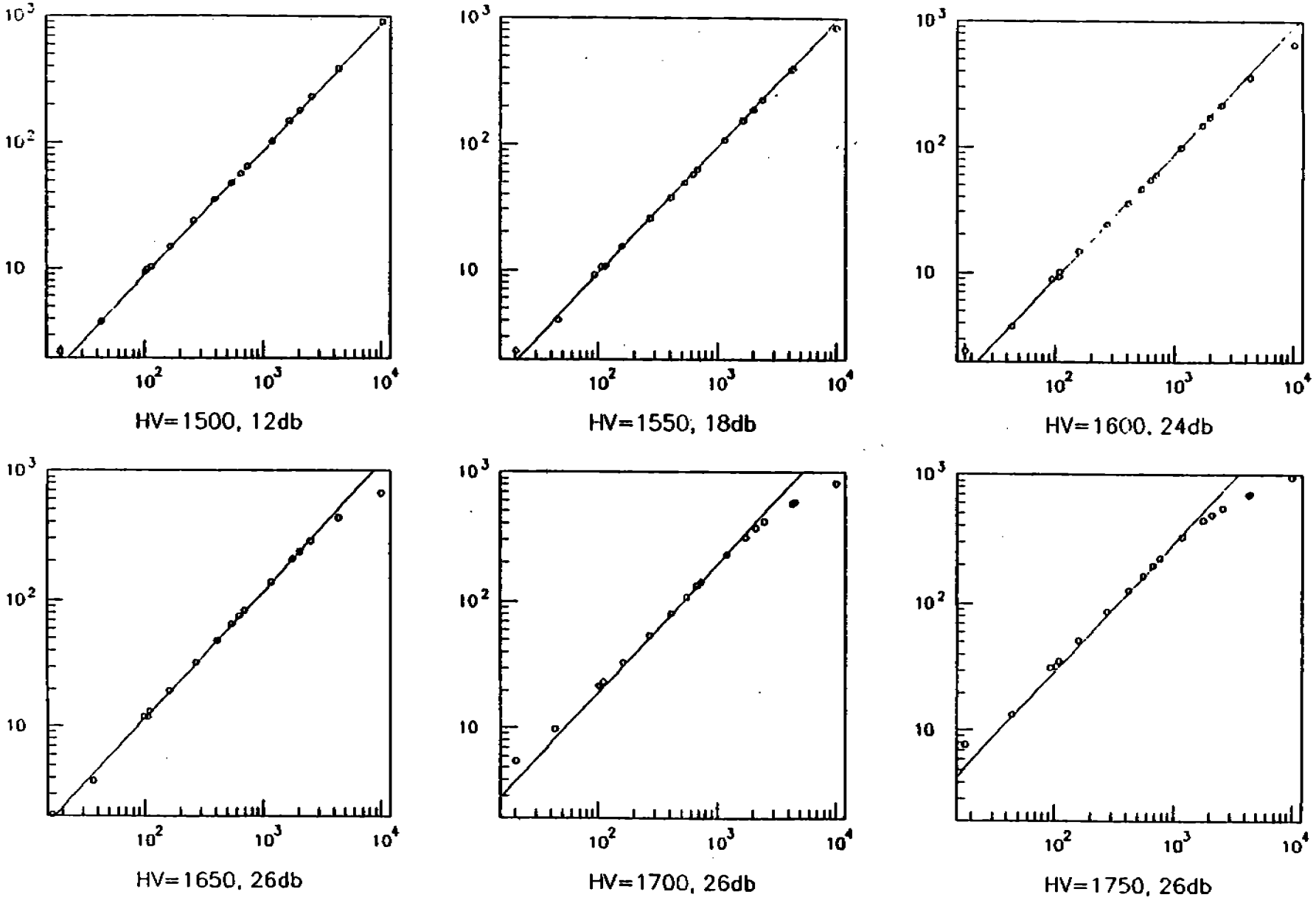

Figure 7: Amplitude: Tested PMT vs Pe's

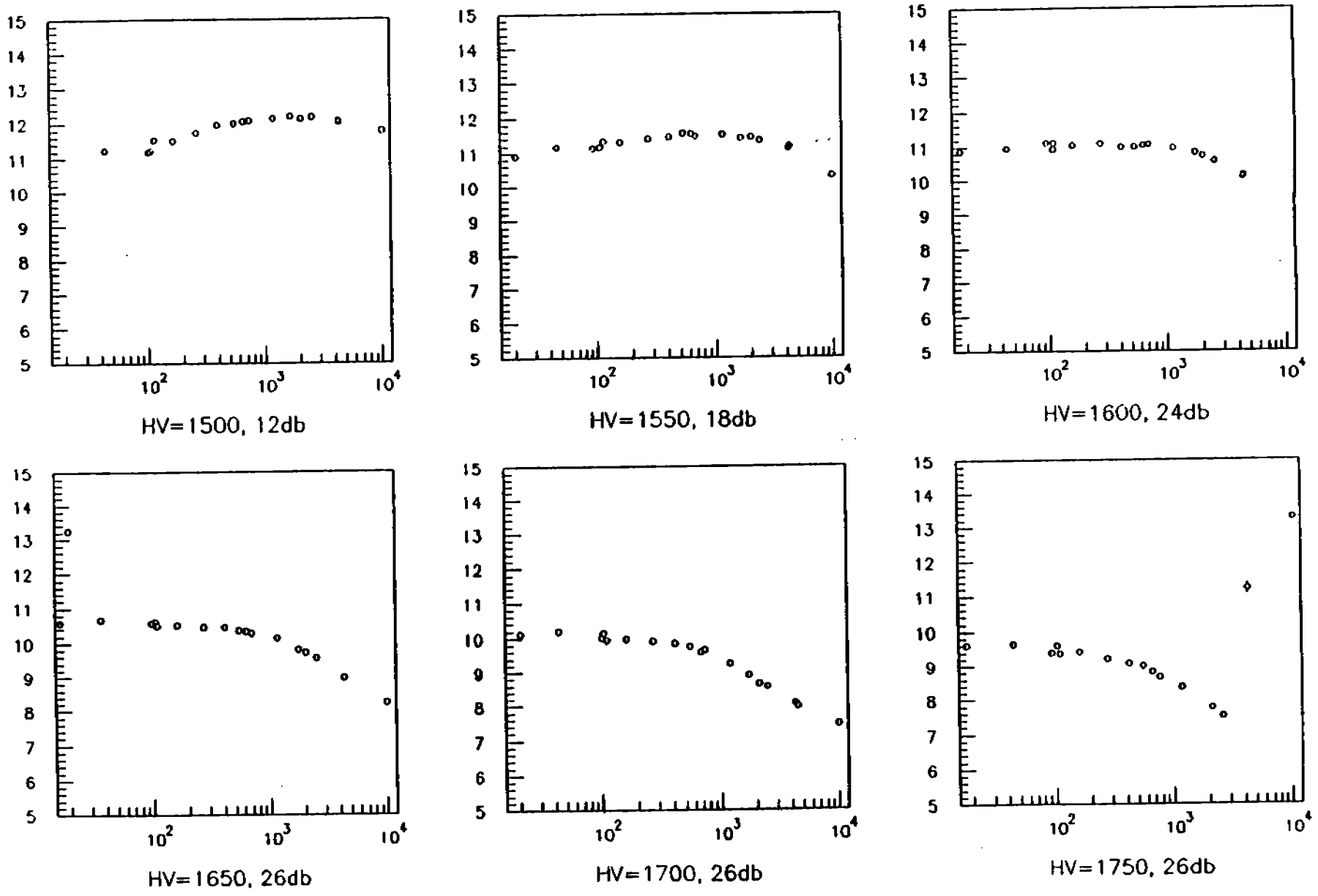

Figure 8: Time: Tested PMT vs Pe's

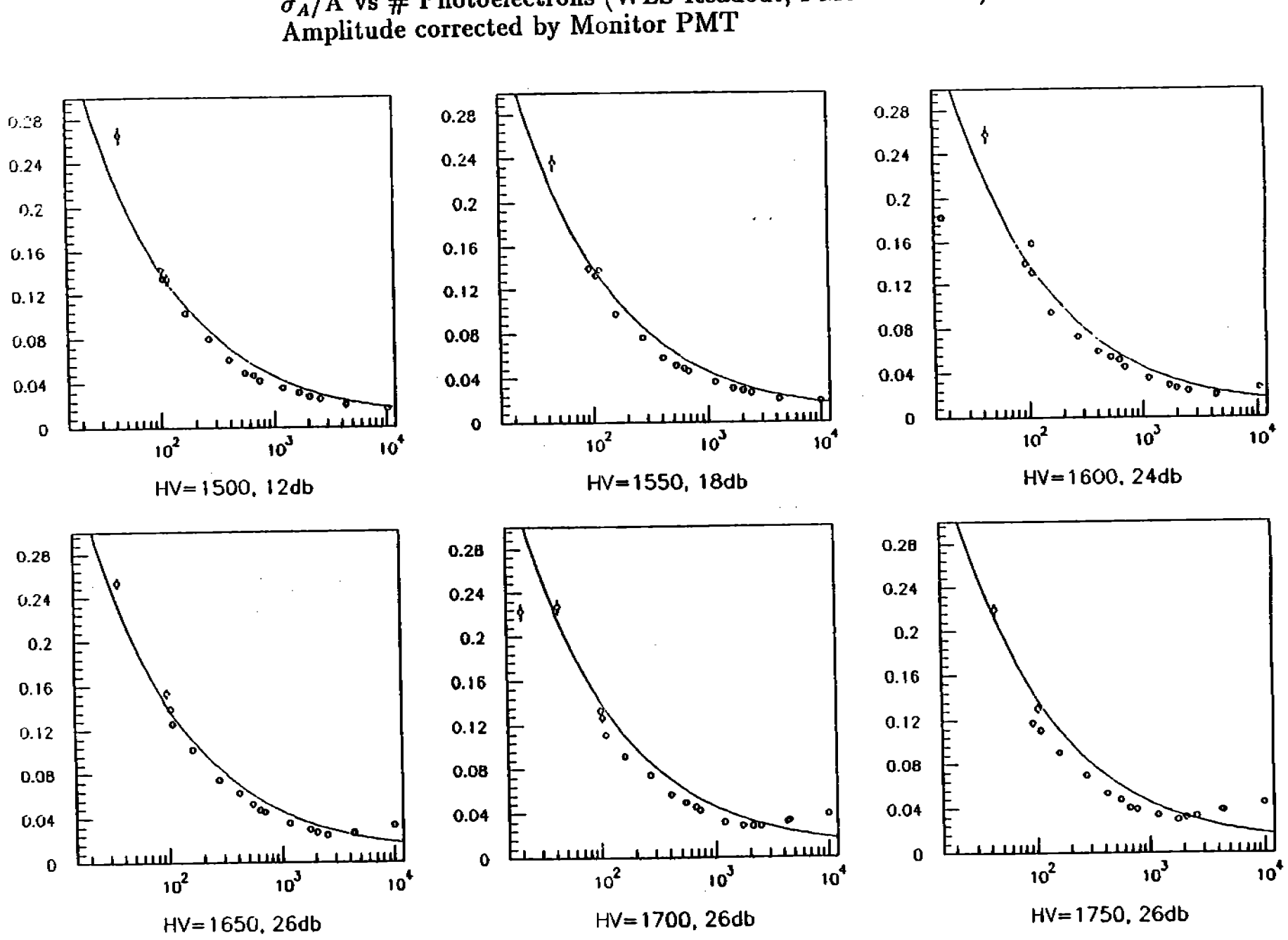

Figure 9: Amplitude Resolution: Tested PMT vs Pe's

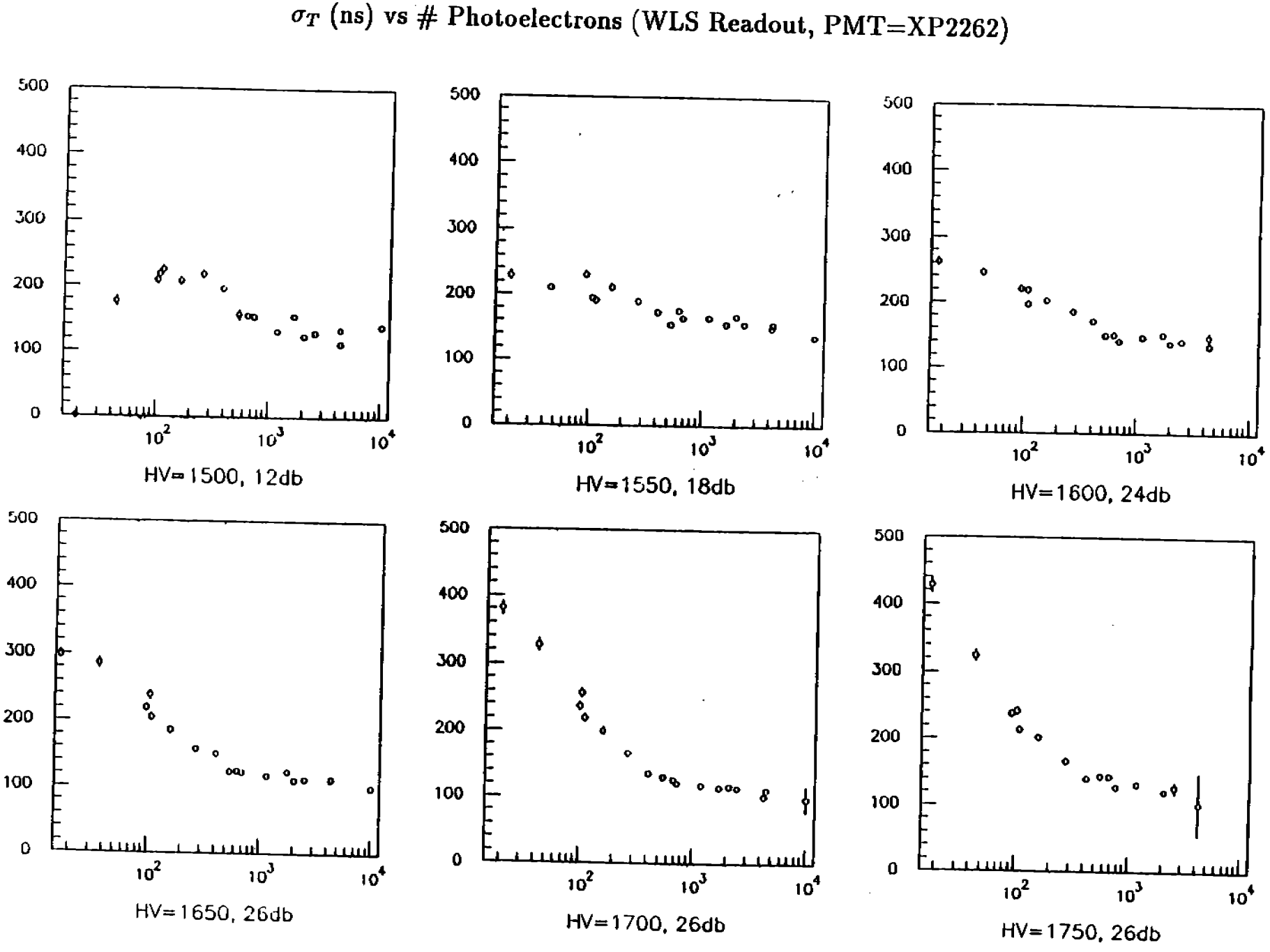

Figure 10: Time Resolution: Tested PMT vs Pe's

TESTED TUBES

FIBER READOUT METHOD

Type	N-stage	Rise time ns	Linearity	N Ph-e, from 1 MeV *	Time res. ns A1	Time res. ns A2	Ampl res. A1	Ampl res. A2	HV
PHILIPS									
XP 2212 (1)	12	4.0	E.....	5.8+/-1.1	1.706	0.045	0.931	0.009	1550
XP 2212 (2)	12	4.0	E.....	5.1+/-0.8	1.673	0.012	1.027	0.008	1550
XP 2262 (1)	12	2.0	..G....	6.2+/-0.8	1.474	0.042	1.005	0.013	1600
XP 2262 (2)	12	2.0	..G....	5.2+/-0.7	1.225	0.053	1.065	0.005	1600
XP 2282	8	1.5	..G....	6.3+/-1.5	1.251	0.049	1.101	0.007	2050
HAMAMATSU									
H 1161 (1)	12	2.7	..G....	6.4+/-0.5	1.490	0.041	1.026	0.001	1450
H 1161 (2)	12	2.7	..G....	6.6+/-0.4	1.581	0.028	0.949	0.008	1450
H 3178 (1) 1.5 inch	10	2.7	E.....	7.3+/-0.7	1.940	0.038	0.943	0.005	1450
H 3178 (2) 1.5 inch	10	2.7	E.....	7.0+/-0.7	2.023	0.047	0.931	0.009	1450
EMI									
9954 B (1)	12		..G....	4.7+/-0.5	1.807	0.028	0.978	0.020	1750
9954 KB (2)	12		E.....	6.7+/-0.6	1.685	0.032	1.047	0.010	1550
9954 KB (3)	12		E.....	7.4+/-0.2	1.435	0.038	1.094	0.009	1500
9939 KB (1)	12		E.....	7.7+/-0.4	1.861	0.033	1.009	0.011	1450
9939 KB (2)	12		E.....	6.6+/-1.1	1.403	0.044	0.920	0.009	1500
9266 KB (1)	10		..G....	6.2+/-0.9	3.630	0.066	0.919	0.008	1450
9266 KB (2)	10		..G....	6.4+/-0.4	3.581	0.028	0.937	0.012	1450
9902 KB (1) 1.5 inch	10		....F..	6.5+/-0.7	2.607	0.062	1.076	0.015	1200
9902 KB (2) 1.5 inch	10		....F..	6.4+/-0.7	3.733	0.053	1.064	0.011	1100
BURLE									
8575	12	2.8	......P	5.8+/-1.1	2.021	0.054	1.081	0.018	2050

E - excelent, G - good, F - fair, P - poor.

Table 5: Tabulted Results for the fiber Readout Tests

methods.

Table 6: Number of Photoelectrons

Losses	Percent Remaining		no. photons Remaining	
	WLS	Fibers	WLS	Fibers
Intial 1 MeV			10000	10000
Total Internal Reflection	18%	18%	1800	1800
Attenuation	72%	72%	1300	1300
Transmitted to WLS	50%		650	
Transmitted to Fiber		10%		130
Absorbed in WLS	80%		520	
Reflected through fiber		25%		32
Reflected through WLS	18%		94	
Attenuation in WLS	80%		75	
Quantum Efficiency	13-10%	25%	9	8

4 Conclusion

Several tests were performed on a set of candidate PMTs in order to understand the limits imposed by PMTs on the performance of the EMC detector. These tests served as a guide for specifying requirements for the procurement of PMTs. A full compilation of the results is available.

A TOF Measurement for Neutrons

The EMC detector will be used to measure neutron velocities. Neutrons will have energies that range from a few hundred Mev to several GeV. At low energies a measurement of the velocity can be used to determine the neutron kinetic energy. At high energies the relativistic kinetic energy is not well determined by a velocity measurement. However, an accurate determination of the neutron velocity can be used to separate photons from neutrons. The broad spectrum of possible neutron energies produces considerable variation in the response of the EMC detector to neutrons. The ability to determine the flight time and the flight path for a given neutron will subsequently also vary considerably. Neutrons, for example, that fail to produce signals in at least two views (U, V, W) will have large timing errors. These errors result when corrections based on the neutron interaction point cannot be applied. High energy neutrons can deposit large amounts of energy. They will have a high probability of producing a signal in all three views and should produce a large number of photons. An accurate velocity measurement should therefore be possible. There are a class of such neutron signals that are detected under optimal conditions and therefore have minimal TOF errors. It is these neutron events that determine the required level of performance for the EMC components. This appendix will use these neutron events to examine the timing of the EMC detector.

The error in the measured velocity is due to the uncertainty in the flight path and the flight time. Because the neutrons coming from the target have relatively small angles with respect to the surface normals, flight path uncertainty results predominantly from an inability to determine the longitudinal location of the neutron interaction in the detector. The flight time uncertainty combines errors due to the neutron trajectories with the intrinsic timing uncertainty of the detector [e]. For this discussion, the point of interaction within a submodule is considered to be completely unknown. Analysis methods that might restrict the point of longitudinal interaction have not been considered. After the neutron interacts the light signal must

[e] In this report intrinsic timing error will refer to the error resulting if only neutrons with identical trajectories and identical interactions depths were to be measured.

propagate to the photomultiplier tubes. This propagation distance will depend on the longitudinal neutron interaction point for two reasons. Firstly, because neutrons travel at an angle with respect to the longitudinal direction they will have different transverse interaction positions as a function of the neutron interaction depth. Secondly, the scintillators in a given submodule increase in length in going from inner to outer scintillators. For neutrons coming from the target these two effects are opposite when the neutron interacts close to the readout end of a scintillator and additive when the neutron interacts far from the readout end. At points close to the readout end the scintillators increase in length so as to compensate for the transverse motion of the neutrons that come from the target. The distance to the end of the scintillator is then independent of interaction depth. The total light path, however, includes both the scintillator path as well as the transport of the light from the scintillator to the photomultiplier tube. The total light path is then greater for the inner scintillators. As discussed below, this light path difference compensates, to some degree, for the additional flight time of the neutron when it interacts later in its path through the EMC detector. At the point furthest from the readout end the light path is minimally dependent on the interaction point. Interactions that occur in the outer scintillators have longer light paths in the scintillator but shorter paths from scintillator to photomultiplier tube. For the longest scintillators the light paths for inner and outer scintillators are approximately equal when the neutron interaction is at the furthest point from the readout end. The flight path uncertainty is maximum for these events (ie no compensation).

To understand the compensation mentioned above the path that the light travels can be broken into a transverse path and a longitudinal path. The iongitudinal part of the light path should be considered in conjunction with the uncertainty in neutron longitudinal interaction point, σ_{path}. The sum of these two longitudinal distance is approximately a constant. The uncertainty then comes from the difference between the neutron speed and the propagation speed of the light in the scintillator. These two effects are combined as σ_{path}.

$$\sigma_{path} = (1.5\beta_n - 1)(\Delta L)$$

v_n is the neutron velocity, 1.5 is the index of refraction of plastic, L is the distance from the target to the final layer in the detector and Δ L is the uncertainty in the neutron interaction location. Note that when the neutron velocity is equal to the speed of light in plastic the above expression for σ_{path} is zero.

The remaining uncertainty in the velocity is σ_{time}. In order to understand the limits on this uncertainty imposed by the readout system the neutron interaction must be detected in at least three adjacent layers. This type of event will have the minimum obtainable uncertainty in the measured time because the U, V, and W intersection point can be used as an estimate of the transverse location of the neutron interaction. The U-V-W overlap region is a triangle with sides of roughly 10 cm. A corrected time can be computed based on this transverse position estimate. The error in the corrected time should, therefore, not depend on the transverse neutron interaction location but only on the overall intrinsic time resolution of the EMC detector.

Several important aspects of the problem have not been addressed. Fluctuations that will be introduced through variations in the neutron interaction have not been carefully analyzed. For proton knockout, the angular variation of the outgoing recoil proton will worsen time resolution because the velocity and recoil trajectory will vary. These kinds of variations will be complicated by the presence of the lead layers between scintillators. A general rule of thumb for TOF neutron detection is that the uncertainty in time resolution should be comparable to flight path uncertainty. As indicated the flight path uncertainty for events with U, V and W signals will be less than or equal to .29 meters. This amounts to a few percent for σ/L. The goal will therefore be to keep the intrinsic EMC timing $\sigma = 400ps$.

B Acknowledgements

We would like to express our appreciation for the help we received from the CEBAF staff and a special note of thanks to the CEBAF Detector Group for their help both in terms of resources and useful discussions.

References

[1] V. Burkert, in *Conceptual Design Report, CEBAF Basic Experimental Equipment* (1990).

[2] R. Minehart et al., in *Lead Scintillator Electromagnetic Calorimeter with Stereo Readout* (1990) [CEBAF PR-90-026, Presented at IEEE October 1990].

[3] J. Calarco, in *Research Program at CEBAF III* (1987).

[4] A. van der Berg, in *Research Program at CEBAF III* (1987).

[5] J. Watson, in *Research Program at CEBAF III* (1987).

[6] S. Stepanyan, in *Optical Fiber Readout for the EMC Detector* (1992) [CEBAF CLAS-Note-92-xxx].

[7] R. Bolton et al., Nuclear Instuments and Methods **174**, 411 (1980).